Broadband enhancement of light emission in silicon slot waveguides

Young Chul Jun[1], Ryan M. Briggs[2], Harry A. Atwater[2], and Mark L. Brongersma[1*]

[1]*Geballe Laboratory for Advanced Materials, Stanford University*
476 Lomita Mall, Stanford, CA 94305, USA
[2]*Thomas J. Watson Laboratories of Applied Physics, California Institute of Technology*
Mail Code 128-95, Pasadena, CA 91125, USA
Brongersma@stanford.edu

Abstract: We investigate the light emission properties of electrical dipole emitters inside 2-dimensional (2D) and 3-dimensional (3D) silicon slot waveguides and evaluate the spontaneous emission enhancement (F_p) and waveguide coupling ratio (β). Under realistic conditions, we find that greater than 10-fold enhancement in F_p can be achieved, together with a β as large as 0.95. In contrast to the case of high Q optical resonators, such performance enhancements are obtained over a broad wavelength region, which can cover the entire emission spectrum of popular optical dopants such as Er. The enhanced luminescence efficiency and the strong coupling into a limited set of well-defined waveguide modes enables a new class of power-efficient, CMOS-compatible, waveguide-based light sources.

OCIS codes: (130.2790) Guided waves; (130.0250) Optoelectronics; (140.5680) Rare earth and transition metal solid-state lasers; (230.6080) Sources.

References and links

1. M. Lipson, "Guiding, modulating, and emitting light on silicon – challenges and opportunities," J. Lightwave Technol. **23**, 4222-4238 (2005).
2. B. Jalali and S. Fathpour, "Silicon photonics," J. Lightwave Technol. **24**, 4600-4615 (2006).
3. G. T. Reed, eds. *Silicon Photonics: the State of the Art* (J. Wiley & Sons, West Sussex, England, 2008).
4. Q. Xu, B. Schmidt, S. Pradhan, and M. Lipson, "Micrometre-scale silicon electro-optic modulator," Nature **435**, 325-327 (2005).
5. J. Liu, M. Beals, A. Pomerene, S. Bernardis, R. Sun, J. Cheng, L. C. Kimerling, and J. Michel, "Waveguide-integrated, ultralow-energy GeSi electro-absorption modulators," Nature Photon. **2**, 433-437 (2008).
6. P. M. Fauchet, *Monolithic silicon light sources*, in *Silicon Photonics*, L. Pavesi and D. J. Lockwood, eds., (Springer-Verlag, Berlin, 2004). p. 177.
7. A. Polman, "Erbium implanted thin film photonic materials," J. Appl. Phys. **82**, 1-39 (1997).
8. T. J. Kippenberg, J. Kalkman, A. Polman, and K. J. Vahala, "Demonstration of an erbium-doped microdisk laser on a silicon chip," Phys. Rev. A **74**, 051802(R) (2006).
9. S. Coffa, G. Franzo, F. Priolo, A. Polman, and R. Serna, "Temperature dependence and quenching processes of the intra-4f luminescence of Er in crystalline Si," Phys. Rev. B **49**, 16313-16320 (1994).
10. A. M. Vredenberg, N. E. J. Hunt, E. F. Schubert, D. C. Jacobson, J. M. Poate, and G. J. Zydzik, "Controlled Atomic spontaneous emission from Er^{3+} in a transparent Si/SiO_2 microcavity," Phys. Rev. Lett. **71**, 517-520 (1993).
11. E. Snoeks, A. Lagendijk, and A. Polman, "Measuring and modifying the spontaneous emission rate of erbium near an interface," Phys. Rev. Lett. **74**, 2459-2462 (1995).
12. V. R. Almeida, Q. Xu, C. A. Barrios, and M. Lipson, "Guiding and confining light in void nanostructures," Opt. Lett. **29**, 1209-1211 (2004).
13. Q. Xu, V. R. Almeida, R. R. Panepucci, and M. Lipson, "Experimental demonstration of guiding and confining light in nanometer-size low-refractive-index material," Opt. Lett. **29**, 1626-1628 (2004).
14. J. T. Robinson, C. Manolatou, C. Long, and M. Lipson, "Ultrasmall mode volumes in dielectric optical microcavities," Phys. Rev. Lett. **95**, 143901 (1998).
15. M. Galli, A. Politi, M. Belotti, D. Gerace, M. Liscidini, M. Patrini, L. C. Andreani, M. Miritello, A. Irrera, F. Priolo, and Y. Chen, "Strong enhancement of Er^{3+} emission at room temperature in silicon-on-insulator photonic crystal waveguides," Appl. Phys. Lett **88**, 251114 (2006).

#108537 - $15.00 USD Received 9 Mar 2009; revised 20 Apr 2009; accepted 20 Apr 2009; published 21 Apr 2009

16. M. Galli, D. Gerace, A. Politi, M. Liscidini, M. Patrini, L. C. Andreani, A. Canino, M. Miritello, R. Lo Savio, A. Irrera, and F. Priolo, "Direct evidence of light confinement and emission enhancement in active silicon-on-insulator slot waveguides," Appl. Phys. Lett **89**, 241114 (2006).
17. C. A. Barrios and M. Lipson, "Electrically driven silicon resonant light emitting device based on slot-waveguide," Opt. Express **13**, 10092-10101 (2005).
18. C. Creatore and L. C. Andreani, "Quantum theory of spontaneous emission in multilayer dielectric structures," Phys. Rev. A **78**, 063825 (2008).
19. Y. Xu, R. K. Lee, and A. Yariv, "Quantum analysis and the classical analysis of spontaneous emission in a microcavity," Phys. Rev. A **61**, 033807 (2000).
20. R. Chance, A. Prock, and R. Silby, "Molecular fluorescence and energy transfer near interfaces," Adv. Chem. Phys. **37**, 1 (1978).
21. G. W. Ford and W. H. Weber, "Electromagnetic interactions of molecules with metal surfaces," Phys. Rep. **113**, 195 (1984).
22. A. C. Hryciw, Y. C. Jun, and M. L. Brongersma, "Plasmon-enhanced emission from optically-doped MOS light sources," Opt. Express **17**, 185-192 (2009).
23. E. D. Palik, *Handbook of Optical Constants and Solids* (Academic, Orlando, Fla., 1985).
24. W. L. Barnes, "Fluorescence near interfaces: the role of photonic mode density," J. Mod. Opt. **45**, 661-699 (1998).
25. Y. C. Jun, R. D. Kekatpure, J. S. White, and M. L. Brongersma, "Nonresonant enhancement of spontaneous emission in metal-dielectric-metal plasmon waveguide structures," Phys. Rev. B **78**, 153111 (2008).
26. J.-M. Gerard, *Solid-state cavity-quanum electrodynamics with self-assembled quantum dots*, in *Single Quantum Dots*, P. Michler, ed., (Springer-Verlag, Berlin, 2003). p. 269.
27. E. Burstein and C. Weisbuch, eds., *Confined electrons and photons* (Plenum Press: New York, NY, 1995).
28. L. Novotny and B. Hecht, *Principles of Nano-Optics* (Cambridge Univ. Press: Cambridge, UK, 2006).

1. Introduction

The monolithic integration of photonic and electronic components on the same chip has been envisioned as one of the key enabling technologies for the future telecommunication and electronics industries [1, 2, 3]. Despite impressive progress in photonic components such as modulators and waveguides on CMOS-compatible platforms [4, 5], an on-chip, efficient light source is still missing. Silicon has been the material of choice for the electronics industry, but it is an inefficient light emitter due to its indirect bandgap. Therefore, it is of great importance to identify new ways to accomplish efficient light emitters on a Si-based platform [6]. One promising way is doping silicon (or silica) with rare-earth elements (e.g. erbium (Er^{3+})) [7, 8]. However, due to the long radiative lifetime of the ${}^4I_{13/2}$ to ${}^4I_{15/2}$ transition of Er^{3+}, its emission processes are often susceptible to nonradiative recombination and quenching processes (e.g. concentration quenching) [9]. Therefore, increasing the spontaneous emission rate of Er [10, 11] is important for improving luminescence efficiency or minimizing the effects of quenching processes, possibly allowing for a higher doping density.

Recently, a novel waveguide structure confining light in a very thin low index slot region was proposed [12, 13]. This slot waveguide consists of a nanometer-sized low index region (e.g. SiO_2) in between two high index regions (e.g. Si). Due to the continuity of the displacement (D) field, the low index slot region can obtain a large E field intensity for the transverse magnetic mode. It was also noted theoretically that this enhanced field strength and confinement can improve light emission in slot-based cavity structures via a reduced mode volume V_m – note Purcell factor in a cavity ~ Q/V_m [14]. Several experiments [15, 16] and theoretical work [17] investigated light emission in silicon slot structures. However, it is not thoroughly studied how lifetime of optical dopants (e.g. Er in SiO_2) is modified in realistic 2D and 3D slot waveguide configurations. In addition, the waveguide coupling ratio of emitted light is not investigated, which is another important factor for achieving power-efficient, on-chip light sources.

In this paper, we investigate the performance of planar (2D) and wire-like (3D) silicon slot waveguides as an integral component of an on-chip light source and obtain the spontaneous emission enhancement (F_p) and waveguide coupling ratio (β) for optical dopants in the low index slot region. For planar 2D silicon slots, we present results from analytical solutions that are in agreement with and further add to recent quantum mechanical studies on doped planar multilayer structures [18]: C. Creatore and L. C. Andreani, "Quantum theory of spontaneous

#108537 - $15.00 USD Received 9 Mar 2009; revised 20 Apr 2009; accepted 20 Apr 2009; published 21 Apr 2009

emission in multilayer dielectric structures," Phys. Rev. A 78, 063825 (2008). For 3D structures, we present both purely numerical results (from 3D finite difference time domain (FDTD) simulations) and semi-analytical results (from Fermi-golden rule calculations). We find that a greater than 10-fold enhancement of F_p can be achieved, together with a β as large as 0.95. In contrast to the case of high Q optical resonators, such performance enhancements are obtained over a broad wavelength region, which can cover the entire emission spectrum of popular optical dopants such as Er in SiO_2. This results in enhanced luminescence efficiency and the strong coupling of emitted light into a limited set of well-defined waveguide modes. These observations are important for realizing a new class of power-efficient, CMOS-compatible, waveguide-based efficient light sources.

2. Planar (2D) silicon slot waveguides

It is well known that the dielectric environment of an emitter can dramatically affect its radiative decay rate. The modifications in the spontaneous emission (SE) rate can be obtained by calculating the emitted power from a classical dipole source [19, 20, 21, 22]. This is also equivalent to calculating the work done on a dipole by its own reflected field. For multiple dielectric layers, an analytic formula for the reflected field and SE rate can be obtained through a plane-wave decomposition and successive applications of the Fresnel reflection coefficients. For a general 5-layer system describing a planar slot waveguide with a dipole in the center layer, the normalized radiative decay rates for normal and parallel dipoles can be expressed as follows [21]:

$$\frac{\gamma_\perp}{\gamma_3} = \frac{3}{2}\mathrm{Im}\int_0^\infty du \frac{u^3}{\ell_3}\frac{[1+r_{345}^{\parallel}e^{-2\ell_3\hat{s}}][1+r_{321}^{\parallel}e^{-2\ell_3\hat{d}}]}{1-r_{321}^{\parallel}r_{345}^{\parallel}e^{-2\ell_3\hat{W}}} \quad (1a),$$

$$\frac{\gamma_\parallel}{\gamma_3} = \frac{3}{4}\mathrm{Im}\int_0^\infty du \frac{u}{\ell_3}\{\frac{[1+r_{345}^{\perp}e^{-2\ell_3\hat{s}}][1+r_{321}^{\perp}e^{-2\ell_3\hat{d}}]}{1-r_{321}^{\perp}r_{345}^{\perp}e^{-2\ell_3\hat{W}}} + (1-u^2)\frac{[1-r_{345}^{\parallel}e^{-2\ell_3\hat{s}}][1-r_{321}^{\parallel}e^{-2\ell_3\hat{d}}]}{1-r_{321}^{\parallel}r_{345}^{\parallel}e^{-2\ell_3\hat{W}}}\} \quad (1b),$$

where the indices 1~5 correspond to each layer, $u = k_\parallel / k_3$ and $\ell_j = -i(\varepsilon_j/\varepsilon_3 - u^2)^{1/2}$ are the normalized in-plane and out-of-plane wavevectors, and $k_j = \sqrt{\varepsilon_j}\omega/c$. The subscripts $\perp$ and $\parallel$ indicate normal and parallel dipoles. The normalized distances are defined as $\hat{d} = k_3 d$, $\hat{s} = k_3 s$, and $\hat{W} = k_3 W = k_3(d+s)$, where d and s are distances from the dipole to the interfaces, and W is the slot width (i.e. thickness of layer 3). The decay rate is normalized to that of a dipole in a uniform background dielectric medium (γ_3). Here, the 3-layer reflection coefficient $r_{ijk}^{\perp,\parallel}$ is defined as:

$$r_{ijk}^{\perp,\parallel} = \frac{r_{ij}^{\perp,\parallel} + r_{jk}^{\perp,\parallel}e^{-2\ell_2\hat{L}_2}}{1 + r_{ij}^{\perp,\parallel}r_{jk}^{\perp,\parallel}e^{-2\ell_2\hat{L}_2}} \quad (2a),$$

with 2-layer Fresnel reflection coefficients:

$$r_{ij}^{\perp} = (\ell_i - \ell_j)/(\ell_i + \ell_j) \quad (2b),$$

$$r_{ij}^{\parallel} = (\ell_i\varepsilon_j - \ell_j\varepsilon_i)/(\ell_i\varepsilon_j + \ell_j\varepsilon_i) \quad (2c).$$

For an emitter having finite quantum efficiency η_0, the SE enhancements for normal and parallel dipoles are given by:

$$F_p^{\perp,\parallel} = (1-\eta_0) + \eta_0\frac{\gamma_{\perp,\parallel}}{\gamma_3} \quad (3),$$

#108537 - $15.00 USD Received 9 Mar 2009; revised 20 Apr 2009; accepted 20 Apr 2009; published 21 Apr 2009

assuming the nonradiative decay rate is not affected by surrounding dielectric structures. From now on, we consider 5-layer silicon slot structures (inset in Fig. 1(c)) with Er dopants in the center SiO_2 layer. The same formulation can be applied to other types of emitters and dielectric multilayer. We start by assuming that the emitter has unit quantum efficiency (η_0=1) for simplicity. We will consider the effect of finite quantum efficiency at the end of this section. We use tabulated values for the silicon dielectric constant (ε_{Si}) [23], while a dispersionless dielectric is assumed for the SiO_2 layer (ε_{SiO2} = 2.13). For a lossless Si layer (i.e. Im[ε] = 0), the integrand of Eq. (1) has singularities due to waveguide mode excitations. The contributions of those poles might be obtained analytically via the contour integral method, after changing Eq. (1) into a complex domain form. In order to facilitate the numerical integration of them, we instead included the very small imaginary part of the silicon dielectric constant (Im[ε_{Si}] (< 10^{-4}), together with the real part (Re[ε_{Si}]). We find that the introduction of the imaginary part virtually does not change the integration result – i.e. increasing Im[ε_{Si}] by several orders of magnitude does not make a noticeable change in the obtained F_p (less than 1%). We also verified that the same numerical values are obtained as those from the quantum theory [18].

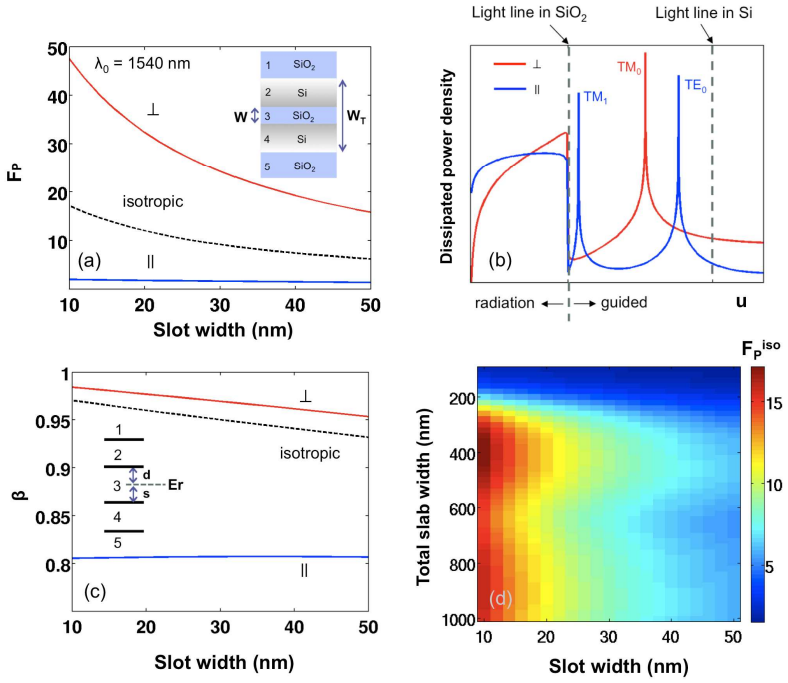

Fig. 1. (a) Spontaneous emission enhancement factor F_p as a function of slot width W. (b) Dissipated power density of a dipole as a function of normalized in-plane wavevector (for W = 20 nm). (c) β as a function of slot width W. Normal and parallel dipoles correspond to red and blue lines, while the isotropic average is shown in a dotted black line. In (a) ~ (c), W_T = 410nm and the red and blue lines correspond to normal and parallel dipoles. (d) Isotroically averaged F_p as a function of total slab width (W_T) and slot width (W). In all cases, we consider a dipole in the middle of the slot and λ_0 = 1540 nm.

Figure 1(a) shows the calculated F_p as a function of slot width (W) for dipoles oscillating normal and parallel to the interfaces, while the total slab thickness W_T is fixed at W_T = 410 nm. We assume that the dipole is in the middle of the slot and its emission wavelength is 1540 nm (i.e. the peak wavelength of Er emission spectrum). F_p for a normal dipole gradually increases as the slot gets thinner, while F_p for a parallel dipole does not change significantly. The integrand of Eq. (1) indicates where the emitted power of the dipole goes and thus it is helpful for understanding the emission enhancement mechanism. As shown in Fig. 1(b) (which is a plot of integrand of Eq. (1) as a function of normalized in-plane wavevector *u* =

#108537 - $15.00 USD Received 9 Mar 2009; revised 20 Apr 2009; accepted 20 Apr 2009; published 21 Apr 2009

$k_{||}/k_3$), a normal dipole couples to the transverse-magnetic (TM) mode (red line), which has strong normal electric field intensity in the slot (due to the D field continuity). Thus we can understand that F_p for a normal dipole increases as the slot width decreases because of the increased TM waveguide mode excitation. A parallel dipole couples to both TE (transverse-electric) and TM modes (blue line). (Note that TM modes have electric field components both normal and parallel to planar interfaces, while TE modes have only parallel electric field components.) However, the parallel electric field components in TE and TM modes are only weakly affected by the presence of the slot, and thus F_p for a parallel dipole is not significantly changed by the slot. Also note that the given structure supports two TM modes and two TE modes. The TE_1 mode peak is not visible in Fig. 1(b), because it has a field node in the center. When we place a dipole off from the center, we see those four modes clearly (Fig. 2(a)).

We also consider a dipole whose orientation is randomly distributed over all directions. The isotropically averaged F_p is obtained by summing one third of the normal dipole enhancement and two thirds of the parallel dipole enhancement [24]:

$$F_p^{iso} = \frac{\gamma^{iso}}{\gamma_3} = \frac{1}{3}\frac{\gamma_\perp}{\gamma_3} + \frac{2}{3}\frac{\gamma_{||}}{\gamma_3} \tag{4}.$$

We find that a slot with W = 20 nm exhibits a larger than 10-fold enhancement in SE, even for randomly oriented dipoles (black dotted line).

Another important factor for efficient light sources is what fraction of emitted light is coupled into the limited set of waveguide modes. We define a waveguide coupling ratio β as the ratio of the waveguide mode excitation rate to the total SE rate from a dipole source.

$$\beta = \gamma_{guided} / \gamma_{total} \tag{5}.$$

As shown in Fig. 1(b), the F_p has two contributions: freespace radiation and guided mode excitation. The region $u < 1$ indicates radiation out of the slab, while the region between the light lines of SiO_2 and Si indicate guided mode excitations. By integrating the relevant wavevector regions, we obtain β for normal and parallel dipoles (Fig. 1(c)). We find that both normal and parallel dipoles have relatively high waveguide coupling ratios ($\beta > 0.8$). A high fraction of the emitted light is trapped inside the silicon slab, owing to the large index contrast between Si and SiO_2 (i.e. via total internal reflection). We also see that a normal dipole has an additional boost resulting from favorable mode profile of the TM modes.

We find that the coupling ratio for isotropically averaged dipole orientations (black dotted line) is still very high - e.g. a 20 nm-wide slot has $\beta^{iso} > 0.95$. The large β ensures that the emitted light is efficiently coupled into waveguide modes.

$$\beta^{iso} = \frac{\gamma_{\perp,guided} + 2\gamma_{||,guide}}{\gamma_{\perp,total} + 2\gamma_{||,total}} \tag{6}.$$

Finally, Fig. 1(d) shows how isotropically averaged F_p changes as a function of total slab width (W_T) and slot width (W). For a fixed slot width W, as the total slab width W_T increases, we observe the oscillation of the SE enhancement appears. The optimized W_T is found to be around 410 nm, which is the thickness we assumed in Figs. 1(a)-1(c).

Figure 2 shows the position dependence of isotropically averaged F_p and β. Fig. 2(b) shows isotropically averaged F_p into individual waveguide modes and radiation mode. It is obtained by integrating relevant in-plane wavevector regions in the dissipated power density spectrum (Fig. 2(a)) and taking the isotropic average (Eq. (4)). As expected from its field enhancement inside a slot, the TM_0 mode excitation dominates over other waveguide and radiation mode excitations. We also see that both F_p and β are nearly constant inside the slot, slightly increasing towards the interface due to the increased field intensity (Figs. 2(c) and 2(d)).

#108537 - $15.00 USD Received 9 Mar 2009; revised 20 Apr 2009; accepted 20 Apr 2009; published 21 Apr 2009

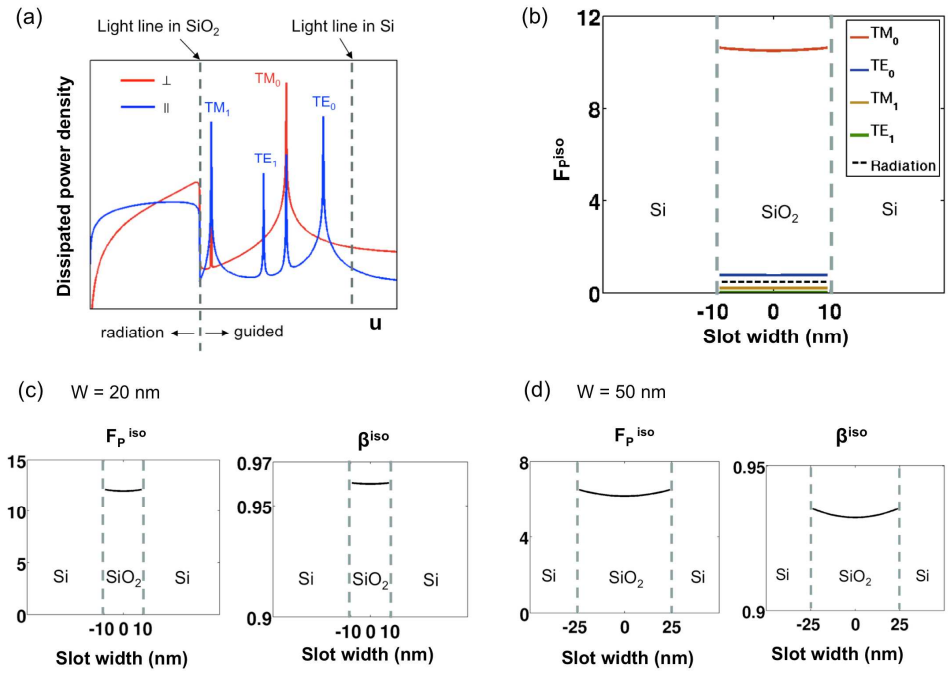

Fig. 2. (a) Dissipated power density of a dipole as a function of normalized in-plane wavevector. The dipole is 5 nm off from the center. (b) Position dependent F_p inside a slot into individual waveguide and radiation modes. Isotropically averaged F_p is plotted. (c), (d) Isotropically averaged, total F_p and β inside a slot. W = 20 nm for (a) ~ (c), and W = 50 nm for (d). In all cases, W_T = 410 nm and λ_0 = 1540 nm.

Figure 3 shows the wavelength dependence of F_p and β for a fixed slot width W = 20 nm. A large enhancement (more than one order of magnitude) is obtained over a whole range of wavelengths. The electric field enhancement and the resultant mode confinement in the slot is mainly determined by the ratio of the dielectric constants in the high and low index regions, so the field enhancement and mode confinement are only very weakly wavelength-dependent. As a result, slot waveguide structures manifest broadband enhancement, which can cover the entire emission spectrum of emitters in the slot (e.g. Er).

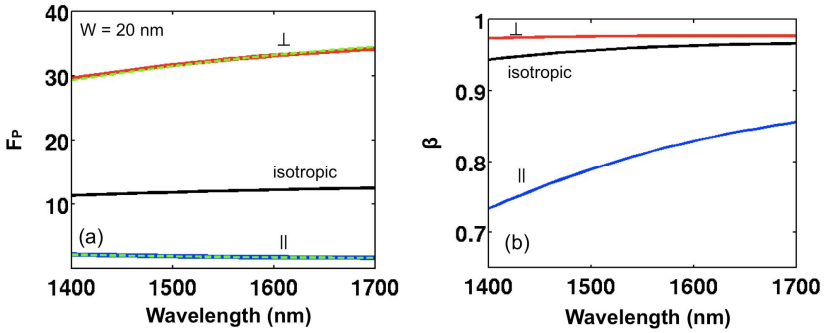

Fig. 3. (a) Spontaneous emission enhancement factor F_p, and (b) waveguide coupling ratio β as a function of the freespace wavelength λ_0 for normal (red line) and parallel (blue line) dipoles. We consider a dipole in the middle of the slot and W = 20 nm. Isotropically averaged values are plotted in black lines. In (a), the result from 3D FDTD simulations are also plotted in green dotted lines.

#108537 - $15.00 USD Received 9 Mar 2009; revised 20 Apr 2009; accepted 20 Apr 2009; published 21 Apr 2009

Now we consider the effect of a finite, initial QE η_0. As shown in Fig. 4(a), the actual enhancement of SE rate is reduced as η_0 decreases. This is because only the radiative decay rate is modified by the dielectric environment. However, with SE enhancement, there is concomitant enhancement of the QE. The isotropically averaged QE η is plotted in Fig. 4(b) as a function of slot width:

$$\eta = \frac{\eta_0 \gamma^{iso} / \gamma_3}{(1-\eta_0) + \eta_0 \gamma^{iso} / \gamma_3} \tag{7}.$$

We find that as the slot width decreases, the final QE increases gradually due to the enhanced waveguide mode excitations. For W = 20 nm, the QE becomes larger than 0.9 for an emitter with initial QE η_0 = 0.5. This efficiency improvement results in a brighter, more power-efficient light source.

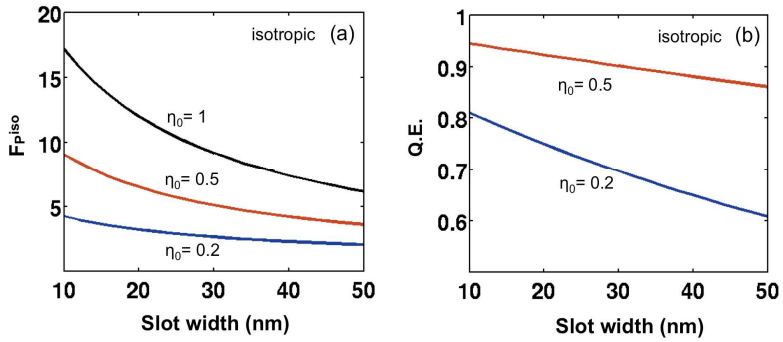

Fig. 4. (a) Isotropically averaged spontaneous emission enhancement factor F_p for different, initial quantum efficiencies. (b) Quantum efficiency (QE) as a function of slot width for two different, initial quantum efficiencies. We consider a dipole in the middle of the slot and λ_0 = 1540nm.

3. Wire-like (3D) silicon slot waveguides

3.1 3D FDTD simulation of total emission enhancement F_p

For a general 3D structure, we cannot set up analytic expressions like Eq. (1), but we can still evaluate F_p and β through numerical methods such as 3D FDTD [19]. The SE enhancement can be obtained by measuring the total outgoing flux from a dipole source and normalizing it by the flux in a homogeneous background dielectric medium (i.e. without structure):

$$F_p = \gamma / \gamma_0 = \langle P \rangle / \langle P_0 \rangle \tag{8},$$

where $\langle P \rangle$ and $\langle P_0 \rangle$ are the time averaged outgoing flux from a dipole with and without dielectric structures.

As a validity check, we first evaluate the total SE enhancement F_p with 3D FDTD for the planar 2D silicon slot structure and compare it with analytic results. To this end, we place a Gaussian dipole source in the middle of the slot. It generates an optical pulse, which covers the whole wavelength region under consideration. After measuring the time-averaged outgoing fluxes, we normalize them by the flux in a uniform dielectric medium (i.e. flux of a dipole embedded in SiO_2). We repeat this simulation for both normal and parallel dipoles and obtain the wavelength-dependence of F_p for orientations. To reduce the computational load, we utilized available symmetries in each case. Fig. 3(a) shows the obtained results from 3D FDTD (dotted lines), together with analytic ones (red and blue lines). We find these methods agree very well (within 1%) over the whole spectrum.

#108537 - $15.00 USD Received 9 Mar 2009; revised 20 Apr 2009; accepted 20 Apr 2009; published 21 Apr 2009

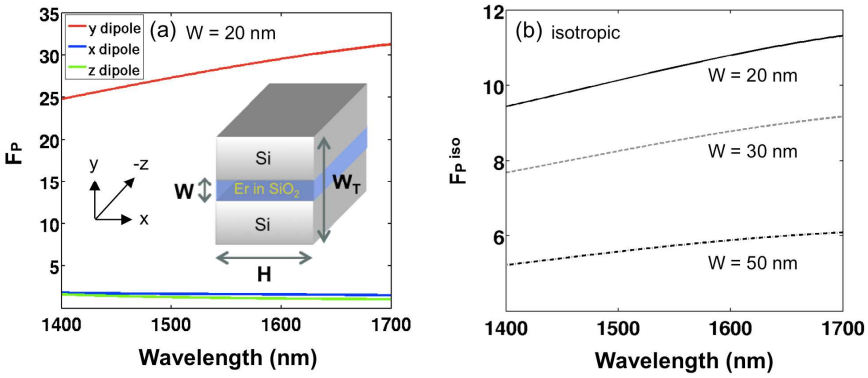

Fig. 5. (a) Spontaneous emission enhancement F_p for a 3D slot structure (W = 20 nm, H = 300 nm, W_T = 410 nm). Red, blue, and green lines correspond to the enhancements from y, x, and z dipoles. (b) Isotropically averaged F_p for slot widths W = 20, 30, 50 nm.

We continued by evaluating F_p for wire-like 3D silicon slots. We adopt the same geometry from Ref. 12: a vertical silicon slot (the inset in Fig. 5) is embedded in SiO_2. It supports the quasi-TE and quasi-TM. The quasi-TE mode has a strong field concentration in the slot region due to the continuity of the D field. But the electric field in the quasi-TM mode is parallel to interfaces and the presence of slot does not significantly affect the field distribution. We place a Gaussian dipole source, oscillating in the x, y, or z direction, in the center of the slot and measured its time-averaged fluxes. Fig. 4(a) shows the obtained total SE rate enhancement F_p. We find that the y-dipole exhibits a much larger enhancement than the x- or z-dipole, similar to 2D planar structures. Figure 4(b) shows the isotropically averaged total emission enhancement factor F_p^{iso} for three different slot widths:

$$F_p^{iso} = \frac{\gamma_{iso}}{\gamma_0} = \frac{\gamma_x + \gamma_y + \gamma_z}{3\gamma_0} \tag{9}.$$

As the slot width decreases, F_p^{iso} increases, due to the enhanced waveguide mode coupling. At the peak wavelength of Er (λ_0 ~ 1540 nm), F_p^{iso} for W = 20 nm is larger than 10-fold. We also observe that the large enhancement is obtained over a broad wavelength range, again similar to 2D slot structures.

3.2 Fermi-golden rule calculation of waveguide mode excitation (F_{wg} and β)

In the previous section, we obtained the total emission enhancement via 3D FDTD, which includes both waveguide mode excitation and freespace radiation. To explicitly get the waveguide mode enhancement F_{wg} and the waveguide coupling ratio β, we derive a simple analytical formula from Fermi-golden rule [25]. This also helps us to obtain a more intuitive understanding for the reasons behind the observed enhancement in waveguide mode excitation.

In the weak-coupling regime, the SE rate of a dipolar emitter can be calculated from Fermi's golden rule:

$$\gamma_{wg}(\vec{r}_e, \omega) = 2\pi \left| g(\vec{r}_e, \omega) \right|^2 D(\omega) \tag{10},$$

where $\left| g(\vec{r}_e, \omega) \right|$ is the coupling strength between the dipole d_0 and the electromagnetic field E at the emitter position $\vec{r}_e$, and D(ω) is the density of states. Assuming the dipole is oriented parallel to the E field, the coupling strength is given by

$$\left| g(\vec{r}_e, \omega) \right|^2 = \left| \vec{d}_0 \cdot \alpha \vec{E}(\vec{r}_e) / \hbar \right|^2 = \omega \left| \vec{d}_0 \right|^2 / \left\{ 2\hbar\varepsilon\varepsilon_0 \tilde{V}_{eff} \right\} \tag{11},$$

#108537 - $15.00 USD Received 9 Mar 2009; revised 20 Apr 2009; accepted 20 Apr 2009; published 21 Apr 2009

where the normalization factor α is

$$|\alpha|^2 = \hbar\omega / \iint \left\{ \varepsilon_0 \frac{d(\varepsilon\omega)}{d\omega} |E|^2 + \mu_0 |H|^2 \right\} d\vec{r} \approx \hbar\omega / \iint 2\varepsilon_0 \varepsilon |E|^2 d\vec{r} \quad (12).$$

We define the effective mode volume as $\tilde{V}_{eff} = \tilde{A}_{eff} \cdot \ell$, where ℓ is an arbitrary quantization length (which cancels out later). We introduce the effective mode area at the emitter position, $\vec{r}_e$, as:

$$\tilde{A}_{eff}(\vec{r}_e) = \frac{\iint \varepsilon_0 \varepsilon(\vec{r}) |E(\vec{r})|^2 d\vec{r}}{\varepsilon_0 \varepsilon(\vec{r}_e) |E(\vec{r}_e)|^2} = A_{eff} \cdot \frac{\max[\varepsilon_0 \varepsilon(\vec{r}) |E(\vec{r})|^2]}{\varepsilon_0 \varepsilon(\vec{r}_e) |E(\vec{r}_e)|^2} \quad (13),$$

Note that the definition of $\tilde{A}_{eff}$ is slightly different from the typical definition of mode area (A_{eff}) in the cavity QED literature [26, 27], where the integrated energy density is divided by the maximum energy density. In the cavity QED community, the Purcell factor is typically calculated using the field at a location of maximum field intensity in a cavity (i.e. antinode position). However, in our case, we place a dipole somewhere inside a slot, which is not necessarily the position of maximum field intensity (or energy density). In quasi-TE mode (or TM mode in case of 2D), the field maximum appears at the Si/SiO_2 interface and the field strength at that interface is determined by the dielectric constant ratio: $\varepsilon_1/\varepsilon_2$. In quasi-TM mode, the maximum energy density point is located inside the silicon region (Fig. 6). For clarity, we introduced the effective mode area at the emitter position. Of course this choice does not change the final enhancement values.

For a wire-like waveguide with a sufficiently small cross sectional area to only have a single TE and a single TM mode, we can assume a 1-dimensional (1D) density of states. The 1D density of states is obtained by counting modes in a 1D space:

$$D(\omega) = \ell / [\pi \upsilon_g(\omega)] \quad (14),$$

where υ_g is the group velocity.

Plugging the equations (11) ~ (14) into Eq. (10), we find the emission enhancement F_{wg} (due to the slot mode excitation) to be:

$$F_{wg} = \frac{\gamma_{wg}}{\gamma_0} = \frac{3}{4\pi} \cdot \frac{c/n}{\upsilon_g} \cdot \frac{(\lambda_0/n)^2}{\tilde{A}_{eff}} \quad (15),$$

where $n = \sqrt{\varepsilon}$ is the refractive index at the source position, and $\gamma_0(\omega) = \omega^3 \sqrt{\varepsilon} |d_0|^2 / (3\hbar\pi\varepsilon_0 c^3)$ is the decay rate in the background medium [28]. λ_0 is the freespace wavelength of the dipole and c is the freespace velocity of light. The above equation shows that the enhancement of waveguide mode excitations comes from group velocity reduction (i.e. density of states) and mode area reduction (i.e. emitter-field coupling strength). To evaluate F_{wg}, we need to know group velocity and effective mode area for a given geometry and wavelength.

We find the group mode index and eigenmode field distribution of a slot waveguide from COMSOL finite element eigenmode solver and obtain the required group velocity and effective mode area for x and y dipoles. Figure 6 shows the eigenmodes for the quasi-TE and quasi-TM modes in 3D silicon slots. The same geometry is used as in the previous section. The quasi-TE mode confines fields strongly in a slot and its electric field is normal to the Si/SiO_2 interface, while the electric field of the quasi-TM mode is distributed over the entire waveguide cross sectional area.

#108537 - $15.00 USD Received 9 Mar 2009; revised 20 Apr 2009; accepted 20 Apr 2009; published 21 Apr 2009

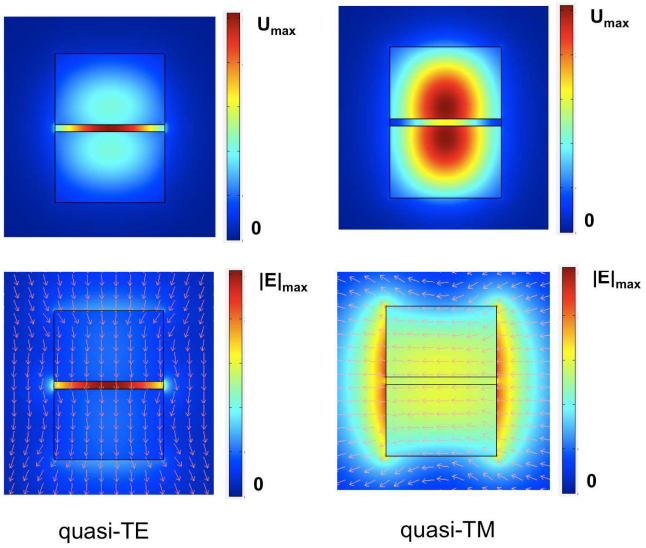

Fig. 6. Eigenmode profiles of quasi-TE and quasi-TM modes in a 3D silicon slot waveguide. Energy density $U=\varepsilon_0\varepsilon|E|^2$ (upper) and Electric field magnitude |E| (lower). Arrows in the lower figures show E-field directions.

First, we compare results from Fermi's golden rule calculation with flux measurement from 3D FDTD simulation as a validity check for this approach. By measuring the flux coupled into the waveguide direction $\langle P_{wg}\rangle$, we can also find a good estimate for $F_{wg} \approx \langle P_{wg}\rangle/\langle P_0\rangle$. The black solid squares and circles in Fig. 7a are the calculated F_{wg} from the Eq (15), shown together with those from 3D FDTD simulation (dotted lines for y, x, and z dipoles). We find both agree quantitatively well over the entire spectral region. The 3D wire-like structures have much larger lateral openings to freespace than 2D structures, but they still have a high waveguide coupling ratio β (Fig. 7(b)). The inset in Fig. 7(b) shows the isotropically averaged waveguide coupling ratio β^{iso} and we find that $\beta^{iso} \sim 0.8$ for W = 20 nm.

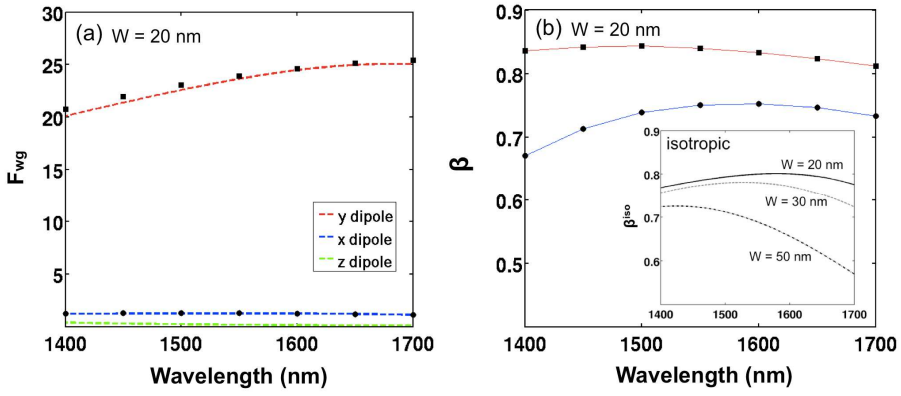

Fig. 7. (a) Waveguide mode excitation enhancement F_{wg} as a function of freespace wavelength. The black solid squares and circles are based on the approach using the Fermi Golden rule (Eq. 15), while the dotted lines from 3D FDTD flux measurements. (b) Waveguide coupling ratio β obtained from the cacluations based on the Fermi Golden Rule. The inset is the isotropically averaged waveguide coupling ratios for three different slot widths. W = 20 nm.

#108537 - $15.00 USD Received 9 Mar 2009; revised 20 Apr 2009; accepted 20 Apr 2009; published 21 Apr 2009

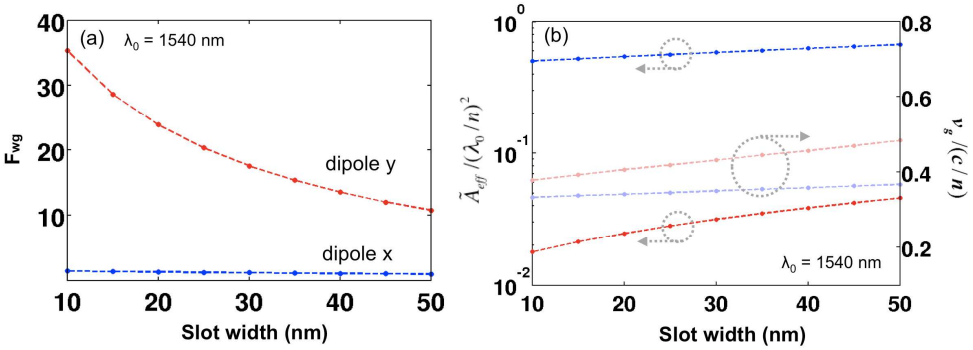

Fig. 8. (a) Waveguide mode excitation enhancement F_{wg} as a function of slot width. (b) Normalized effective mode area and mode group velocity as a function of slot width. W = 20 nm.

Figure 8(a) shows the calculated enhancement factor F_{wg} as a function of the slot width. Similar to the 2D case, F_{wg} for a y-oriented dipole gradually increases, while F_{wg} for an x-oriented dipole does not change much. Figure 8(b) shows that the larger enhancements at small slot widths find their origin in reduction of both the group velocity and the mode area. However, we find that the group velocity changes only modestly and the major reason for the large enhancement in the y-dipole emission is related to the reduced mode area. The reduced mode area generates a stronger field at the source position and eventually resulting in an increased coupling between the dipole and the waveguide mode.

Finally, we evaluate the position-dependent enhancement inside a 3D slot. Figure 9 shows the position-dependence of the enhancement for x- and y-dipoles (i.e. a F_{wg} map). Note that different color scales are used for the quasi-TE and quasi-TM modes. We find that the quasi-TE mode exhibits a much larger waveguide mode excitation enhancement over the entire slot area. F_{wg} for a y-dipole is very high in the center of the slot and even the averaged F_{wg} over the entire slot area is significant (~ 18.3 for a y-dipole).

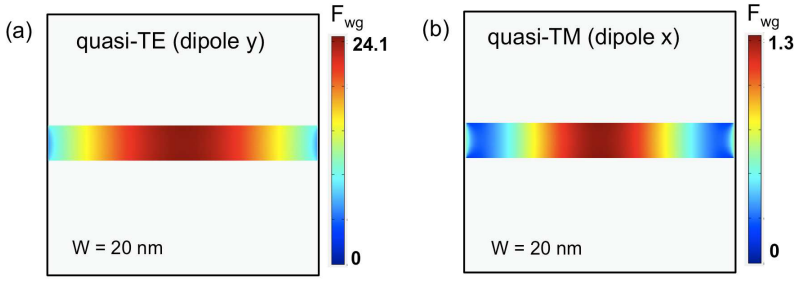

Fig. 9. F_{wg} map inside a W = 20 nm slot for (a) y-dipole (which couples to quasi-TE mode) and (b) x-dipole (which couples to quasi-TM mode). λ_0 = 1540 nm.

4. Conclusion

We investigate the light emission properties of electrical dipole emitters in planar (2D) and wire-like (3D) silicon slot waveguide structures. Both the spontaneous emission enhancement (F_p) and waveguide coupling ratio (β) for optical dopants in the low index slot region (e.g. Er in SiO_2) were quantified for a range of design parameters. For planar 2D silicon slots, we present results from analytical solutions. For 3D structures, we use 3D FDTD simulations and a semi-analytical equation (based on Fermi-golden rule) to evaluate F_p and β. We find that the strong confinement of fields in the slot enables a greater than 10-fold enhancement of F_p, together with a large β factor. This is achieved over a broad wavelength range, which can

#108537 - $15.00 USD Received 9 Mar 2009; revised 20 Apr 2009; accepted 20 Apr 2009; published 21 Apr 2009

cover the entire emission spectrum of popular optical dopants. This effect can be used to boost the luminescence efficiency of slow emitters and to enable efficient coupling of light into a limited set of well-defined waveguide modes. These findings are important for the realization of CMOS-compatible and power-efficient light sources.

Acknowledgments

The authors wish to thank Thomas Koch and Gernot Pomrenke for helpful discussions. Y.C.J. acknowledges the support of the Samsung scholarship. R.M.B. acknowledges the support of the National Defense Science and Engineering Graduate Fellowship. This work was supported by Si-based Laser Initiative of the Multidisciplinary University Research Initiative (MURI) under the Air Force Aerospace Research (Award No. FA9550-06-1-0470).

#108537 - $15.00 USD Received 9 Mar 2009; revised 20 Apr 2009; accepted 20 Apr 2009; published 21 Apr 2009